Evaluation of Bridging Characteristics in Fiber-Reinforced Cementitious Composite Considering Fiber Rupture Probability

(繊維の破断確率を考慮した繊維補強セメント複合材料の架橋性能評価)

TIAN WEICHAO

(Master's Program in Engineering Mechanics and Energy)

Advised by Toshiyuki Kanakubo

Submitted to the Graduate School
of Science and Technology
Degree Programs in Systems and
Information Engineering
in Partial Fulfillment of the Requirements
for the Degree of Master of Engineering
at the
University of Tsukuba

March 2025

Abstract

Fiber-reinforced cementitious composites (FRCC) are cement-based materials that have been enhanced with fibers to improve their mechanical properties. The fibers are distributed homogeneously within the matrix. In the event of the formation of cracks, the fibers act as bridges, absorbing energy and thereby inhibiting the formation and propagation of cracks. This enhances the mechanical performance of the material, underscoring the importance of understanding fiber bridging behavior for advancing FRCC research.

In this study, a uniaxial tension test was conducted on FRCC with extremely small test areas to investigate thin fibers' single-fiber pullout behavior. By limiting the size of the test area, the influence of fiber orientation is eliminated, allowing for a more accurate assessment of the material's properties. The uniaxial tension test was conducted on 10 specimens for each of the fiber volume fractions of 2% and 3%. The results demonstrated that FRCC with a 3% fiber volume fraction is more prone to exhibiting multiple crack behavior in comparison to FRCC with a 2% fiber volume fraction.

Furthermore, a single fiber pullout model for PVA fiber, incorporating fiber rupture probability, was employed to calculate the bridging law and to facilitate a comparison with the experimental results. The findings indicated that the computational method provided a superior fit for the PVA-2%. However, for the PVA-3%, the fit is less satisfactory due to the pronounced multiple crack behavior observed in the experimental results. The calculated bridging strengths are in close alignment with the experimental tensile strengths in the fiber rupture probability of 0.024 as average. The relationship between fiber rupture probability and bridging strength shows a strong correlation expressed by the derived equation.

Contents

List of Figures

List of Tables

Chapter 1 Introduction

1.1 Research Background

1.1.1 Fiber-Reinforced Cementitious Composite (FRCC)

Fiber-reinforced cementitious composites (FRCC) are a category of cement-based materials designed to enhance mechanical performance through the incorporation of fibers. The classification of fiber-reinforced cementitious composites is shown in Figure 1.1. Conventional cement-based materials, such as concrete, demonstrate remarkable compressive strength but comparatively low tensile strength, typically only approximately one-tenth of their compressive strength. However, the incorporation of fibers markedly enhances tensile properties, particularly in the mitigation of crack formation and propagation.

The addition of fibers to cement-based materials ensures uniform distribution within the matrix. In the event of a developing crack in the FRCC, the fibers act as bridges between fractured matrix sections. This bridging effect allows the fibers to absorb energy, effectively restraining crack propagation. The reduction in crack opening not only enhances the mechanical properties of cement-based materials but also minimizes the ingress of external substances, maintaining structural stability and improving the durability of the material.

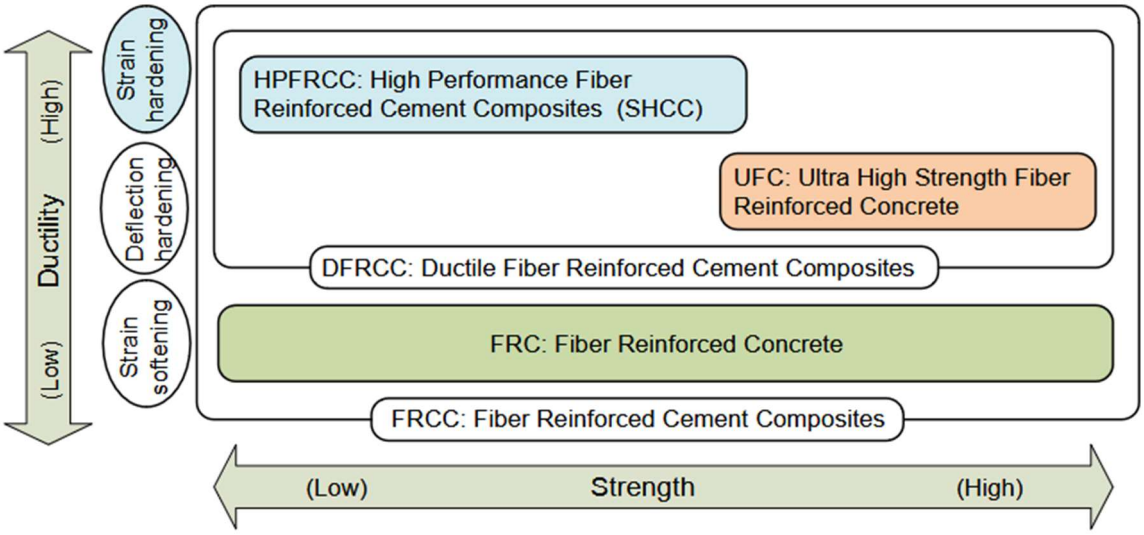

Figure 1.1 Classification of fiber-reinforced cement composites [1]

1.1.2 Pullout Behavior of Single Fiber

To predict and evaluate the bridging effect of fibers, a computational model, known as the bridging law, was proposed. This model establishes a relationship between tensile stress and crack width［2］. The bridging law can be derived using the single fiber pullout model, which is combined with factors such as fiber orientation and dispersion within the matrix, to calculate the relationship between tensile stress and crack width.

As shown in Figure 1.2, the structural behavior of components can be analyzed based on micromechanical parameters, such as fiber properties, matrix performance parameters, and interface characteristics. Micromechanical parameters determine the single fiber pullout model, which subsequently leads to the development of the bridging model. This bridging model describes the behavior of the fiber-bridging effect. By employing the fiber-bridging model, the conditions for multiple crack formation can be derived, forming the basis for a macroscopic material behavior model. This model, in turn, enables the prediction of the structural behavior of components.

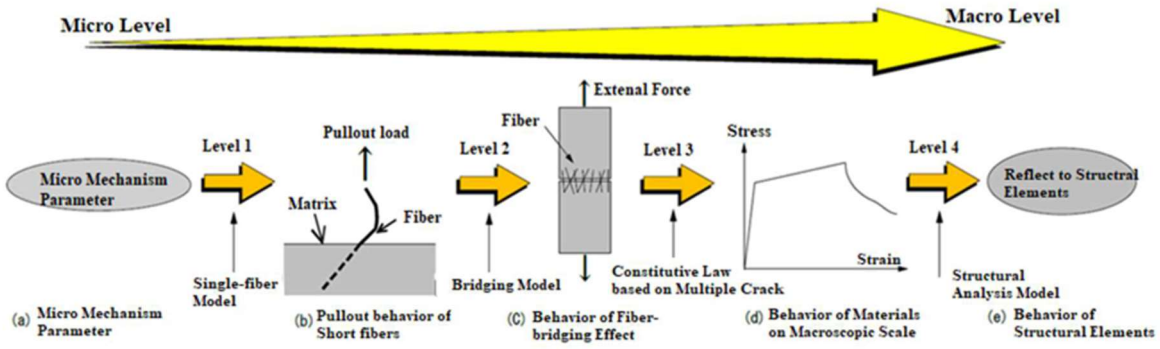

Figure 1.2 The flow of materials design ［3］

1.1.3 Single Fiber Pullout Test

The fiber pullout behavior is influenced by factors such as the inclination angle and embedded length. Therefore, the single-fiber pullout test can be used to derive the single-fiber pullout behavior［4］.

The experimental setup for the single fiber pullout test, as illustrated in Figure 1.3, comprises a specimen in which the fiber is embedded in the matrix. The length of the fiber embedded in the matrix is regulated by modifying the thickness of the matrix. Subsequently, the matrix is secured to the testing machine with an acrylic plate, as illustrated in Figure 1.4, and the inclination angle of the fiber is calibrated to attain the desired fiber orientation. This single-fiber pullout test enables the formulation of the single-fiber pullout model.

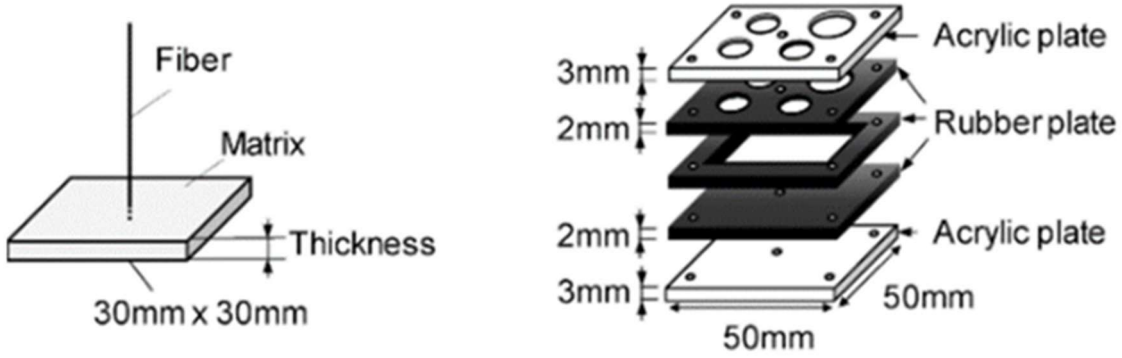

Figure 1.3 Specimen for pullout test［5］

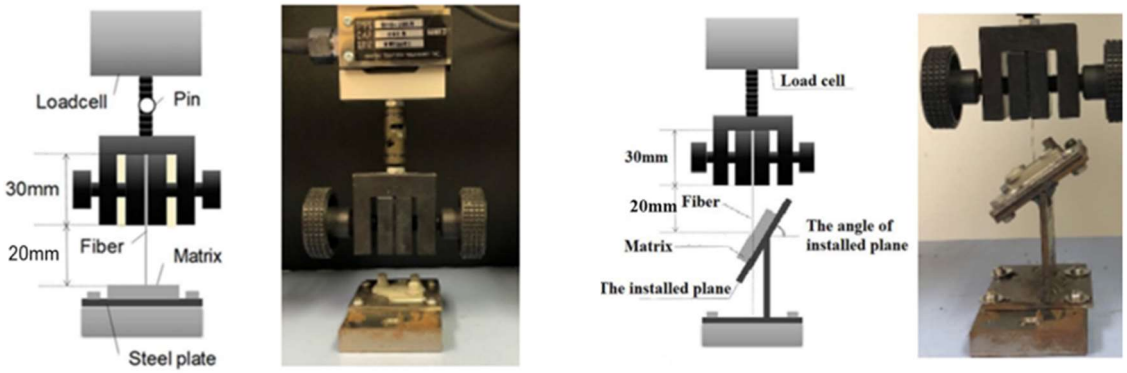

(a) specimen at 0 inclination angle (b) specimen with inclination angle

Figure 1.4 Pullout test setup［5］

Two potential outcomes may arise during the fiber bridging process: fiber pullout or rupture. The primary cause of fiber rupture is attributed to the apparent strength of the fiber and its inclination angle. The inclination angle introduces a snubbing effect, which increases the difficulty of fiber pullout and reduction of the fiber rupture strength［5］. When the bridging strength exceeds the fiber's strength, rupture occurs. The apparent strength of the fiber depends not only on the intrinsic strength of the fiber but also on its dimensions. Therefore, studying the influence of fiber size on the pullout behavior in FRCC is crucial for understanding its performance.

In general, single-fiber pullout testing with fiber diameters less than 0.1 mm is challenging due to difficulties in specimen preparation and experimental execution. As shown in Table 1.1, although the types of fibers vary widely in previous studies, the fiber diameters are typically larger than 0.1 mm to facilitate specimen preparation and testing. When the fiber diameter is smaller than 0.1 mm, embedding the fiber in the matrix becomes problematic due to the extremely fine nature of the fiber, making it difficult to perform single-fiber pullout experiments.

Table 1.1 Fiber dimensions for single fiber pullout test in previous research

Authors	Fiber Type	Diameter	Length
Abrha, S.F. et al.［5］	Palm fiber	Over 0.12 mm	Over 5 mm
Kanakubo, T et al.［6］	Bundled aramid fiber	0.5 mm	30 mm
Hashimoto, H. et al.［7］	Polypropylene fiber	0.7 mm	30 mm
Echizen, S. et al. ［8］	Steel fiber	0.16 mm	13mm

1.2 Research Objective

As previously noted, to gain insight into the pullout behavior of a specific fiber, it is necessary to conduct a single fiber pullout test［4］. However, the implementation of such tests is challenging for thin fibers (generally defined as fibers with diameters less than 0.1 mm), due to the inherent difficulties in specimen fabrication and experimental execution.

The objective of this study is to evaluate the bridging characteristics of fibers in FRCC through uniaxial tension tests under conditions in which fiber orientation factors are excluded. By eliminating the influence of fiber orientation, the only factor affecting fiber bridging characteristics in this experiment is the embedded length. Therefore, this experiment approximates a single fiber pullout test without the influence of fiber orientation (as shown in Figure 1.4), allowing for a simplified analysis of the fiber pullout behavior. The analysis also considers the fiber rupture to evaluate the variations in fiber bridging characteristics.

Chapter 2 Uniaxial Tension Test

2.1 Introduction

In this chapter, the uniaxial tension test is conducted under the condition that fiber orientation factors are excluded to evaluate the fiber pullout behavior. Through these experiments, the tensile load-head displacement relationship and the number of cracks formed in the specimens during loading are observed. A compression test is also conducted to evaluate the compressive strength of cylindrical test pieces.

2.2 Experiment Outline

2.2.1 Applied Fibers

The fiber utilized in this study is polyvinyl alcohol (PVA) fiber, as shown in Figure 2.1. The dimensions and mechanical properties of the fiber are listed in Table 2.1. The fiber used in this experiment has a diameter of 0.1 mm and a length of 12 mm, which classifies them as thin fibers. Furthermore, a previous study has proposed the pullout model of PVA fiber with these dimensions, which allows for the evaluation of the results of this experiment using this model.

Figure 2.1 Photo of applied fiber

Table 2.1 Dimensions and mechanical properties of polyvinyl alcohol (PVA) fiber

Type	Density (g/cm^3)	Diameter (mm)	Length (mm)	Tensile Strength (MPa)	Elastic Modulus (GPa)
PVA	1.30	0.10	12	1200	28

2.2.2 Specimens

The dimensions of the specimens utilized in this experiment are shown in Figure 2.2. The test area of the specimens has a cross-sectional area of 5 mm × 5 mm and a length of 30 mm. The fiber employed in this experiment has a diameter of 0.1 mm and a length of 12 mm. This test area ensures consistent fiber orientation, effectively eliminating the influence of the fiber orientation factor as shown in Figure 2.3.

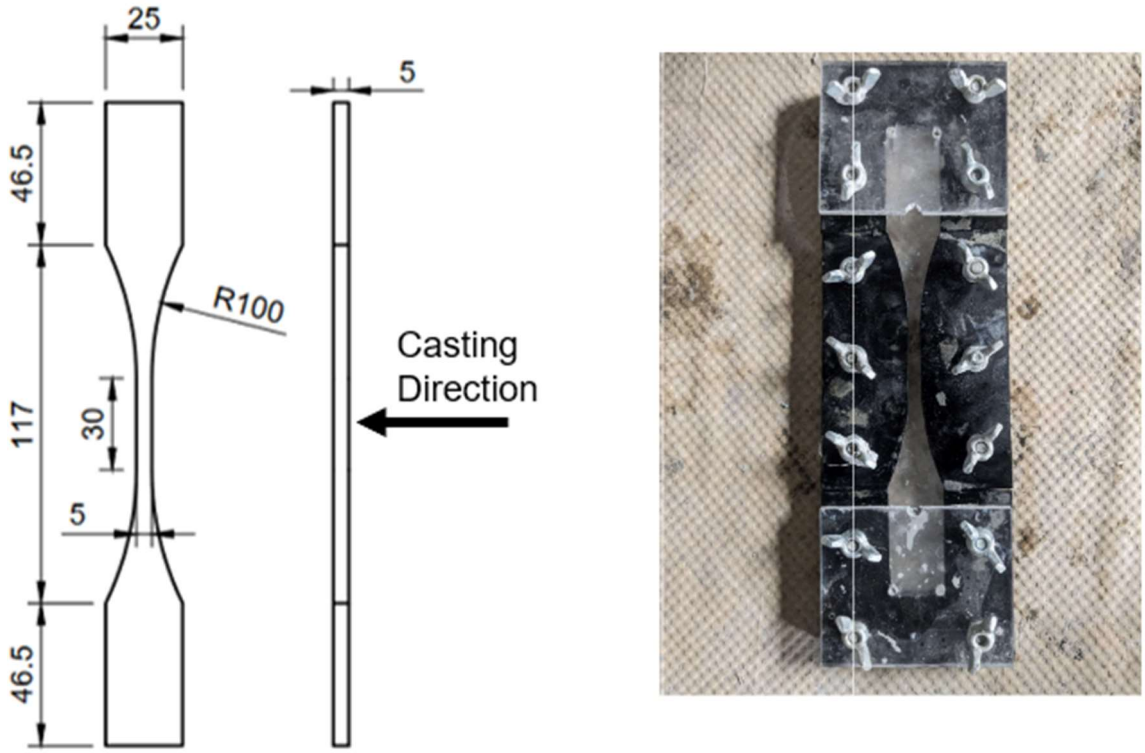

(a) Dimensions of the specimen (b) Mold of specimens

Figure 2.2 Specimens (unit: mm)

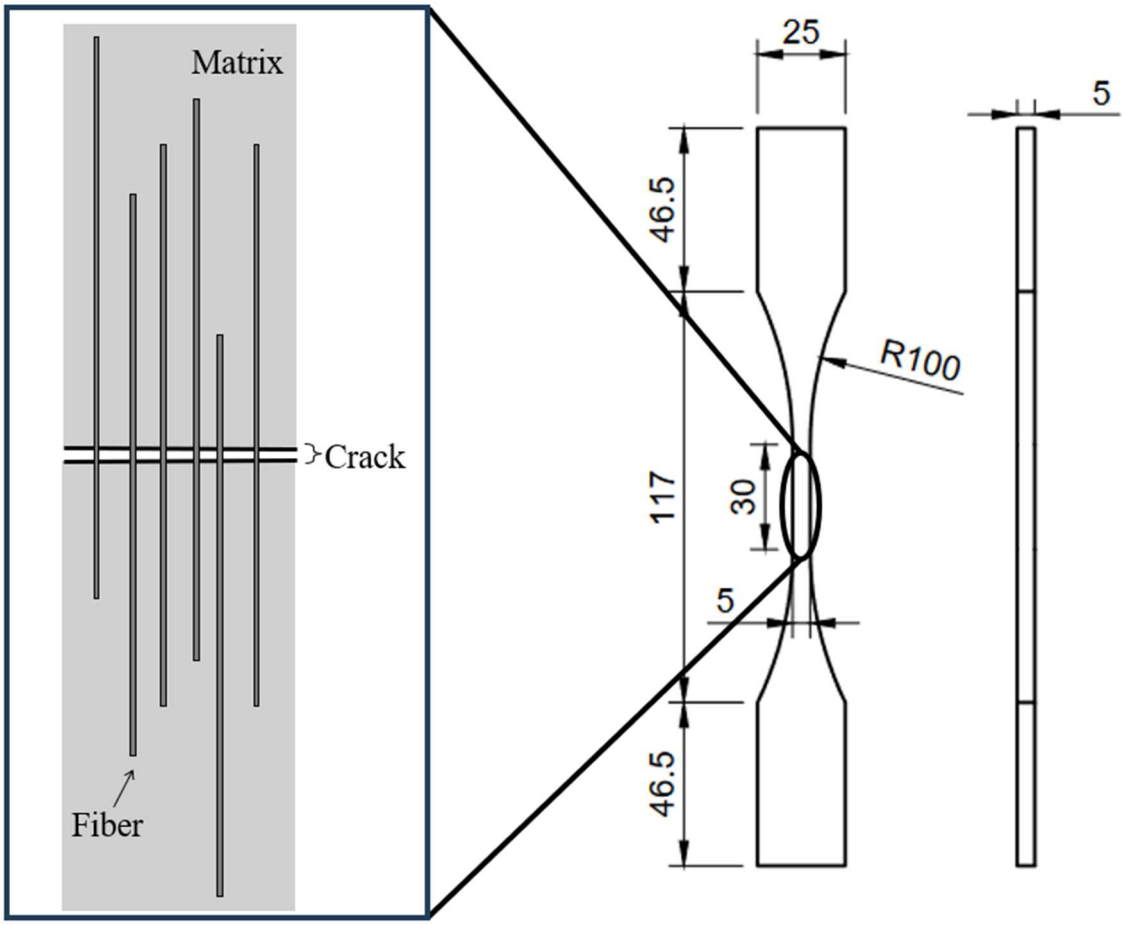

Figure 2.3 Fiber orientation elimination mechanism

2.2.3 Applied Materials

The fiber utilized in this experiment is delineated in Section 2.2.1. The mixture proportion of the FRCC is provided in Table 2.2. Specimens were prepared with two PVA fiber volume fractions (V_f): 2% and 3%. The list of specimens is shown in Table 2.3.

Table 2.2 Mixture proportion of FRCC

W/B	FA/B	Unit weight (kg/m^3)				
		W	C	FA	S	SP
0.39	0.30	380	678	291	484	6

Where:

W: water,

B: binder = (C+FA),

C: high early-strength Portland cement,

FA: fly ash (Type Ⅱ of Japanese Industrial Stand (JIS A 6201))

S: silica sand (size under 0.2mm);

SP: high-range water-reducing agent (=B×0.6%)

Table 2.3 List of specimens

Series	V_f	Number of specimens
PVA-2%	2%	10
PVA-3%	3%	10

2.2.4 Casting Method

The casting procedure for the uniaxial tension test specimens is shown in Figure 2.4. First, FRCC was poured into the test area of the mold (cross-sectional area of 5 mm × 5 mm and 30mm length). Vibration was applied to allow the mortar to flow to both ends of the mold. When the mold was completely filled with mortar, acrylic plates were pressed onto both ends to secure the specimen and ensure that excess FRCC overflowed from the test area.

The specimens were then cured in the air for one day, after which they were immersed in water for further curing. This process includes simultaneously casting cylindrical test pieces for compressive strength tests. After one week of water curing, the specimens were removed from the water, and the hardened overflow mortar in the test area was ground off with an angle grinder. The specimens were then demolded and returned to water cure until the uniaxial tension test was performed.

Casting

Curing

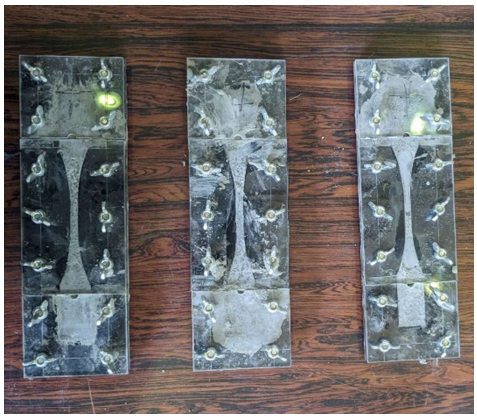

Demolding

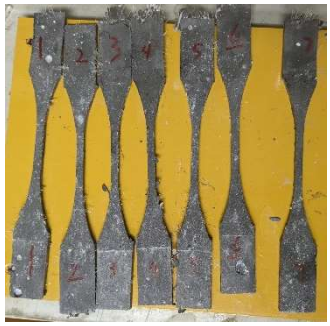

Figure 2.4 Casting method

2.2.5 Loading and Measurement

The uniaxial tension test was conducted using an electronic universal testing machine (LSC-02/30-2, Tokyo Testing Machine Co., Ltd., Tokyo, Japan) with a capacity of 200 N, as shown in Figure 2.5. The loading speed was set at 1 mm/min. Given the limited dimensions of the test area, it proved challenging to install a displacement gauge. Consequently, the experiment yielded the tensile load–head displacement relationship.

Compression test was conducted on the PVA-2% and PVA-3%. The test specimens were cylindrical, with dimensions of φ100 mm ×200 mm. Four specimens were prepared for the PVA-2% and five specimens for the PVA-3%. The compression test was conducted using a universal testing machine with a capacity of 500 kN, as shown in Figure 2.6.

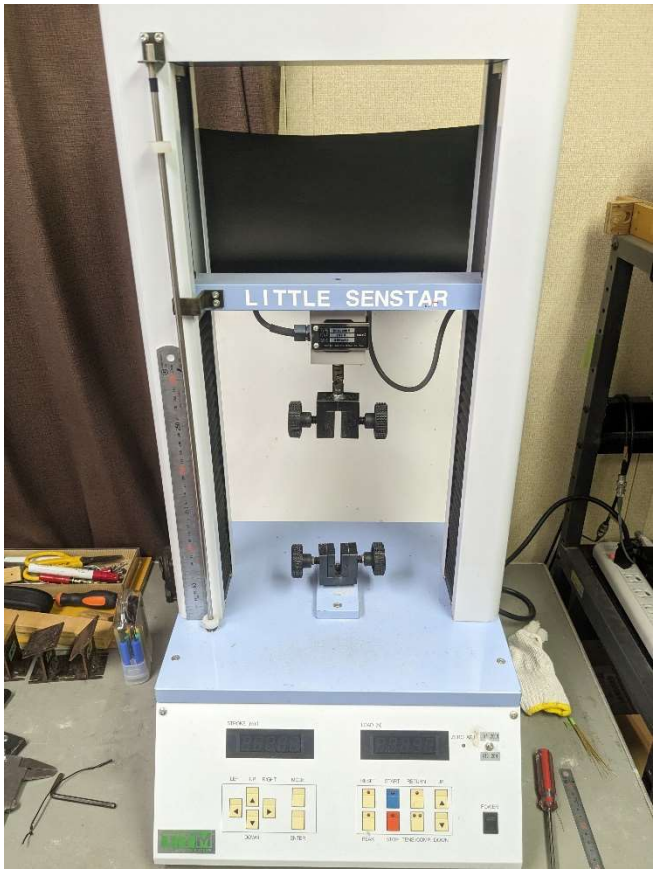

Figure 2.5 Universal testing machine for uniaxial tension test

Figure 2.6 Universal testing machine for compression test

2.3 Experiment Result

2.3.1 Compressive Properties

The compressive strength specimens for the PVA-2% and PVA-3% consisted of four and five cylindrical specimens, respectively, as shown in Figure 2.7. The compressive strength test results are shown in Table 2.4. Both series were cured in water, with the PVA-2% cured for 43 days and the PVA-3% cured for 28 days.

According to the test results, the compressive strength of the PVA-2% was 49.1 MPa, while that of the PVA-3% was 47.7 MPa. This indicates that in the range of fiber volume fractions from 2% to 3%, the compressive strength is not so influenced by the fiber volume fraction.

Table 2.4 Compressive properties

Series	Curing duration (days)	Curing condition	Compressive strength (MPa)	Elastic modulus (GPa)
PVA-2%	43	Curing in water	49.1	19.2
PVA-3%	28		47.7	18.3

Figure 2.7 Photo of the test piece (PVA-2%)

2.3.2 Tensile Properties

For the uniaxial tension tests, 10 specimens were prepared for each of the PVA-2% and PVA-3%, and the demolded specimens are shown in Figure 2.8. Among the PVA-2% specimens, three fractured during the demolding process, while PVA-2%-4 and PVA-2%-5 exhibited cracks before loading. In the PVA-3%, two specimens fractured during demolding and PVA-3%-6 showed cracks before loading. In addition, the ends of the PVA-3%-1 specimen slipped during loading.

Figure 2.8 Photo of specimens (PVA-2%)

The tensile properties of the PVA-2% and PVA-3%, as obtained from the uniaxial tension test, are presented in Table 2.5 and Table 2.6, respectively. The experimental results demonstrate a notable dispersion in head displacement at maximum load for both the PVA-2% and PVA-3%. Similarly, the maximum load values for individual specimens within each series also exhibit considerable dispersion. This is a consequence of the limited extent of the test area.

Despite the observed dispersion, the specimens exhibiting the best performance in both series demonstrated comparable maximum load results. In PVA-2%, specimens PVA-2%-3 and PVA-2%-6 achieved maximum loads of 114.56 N and 107.79 N, respectively. In PVA-3%, specimens PVA-3%-3 and PVA-3%-7 achieved maximum loads of 111.52 N and 118.67 N, respectively. Furthermore, the average tensile strengths of the two series were found to be comparable, with values of 2.54 MPa for the PVA-2% and 2.64 MPa for the PVA-3%.

Table 2.5 Tensile properties (PVA-2%)

ID	Maximum load (N)	Tensile strength (MPa)	Head displacement at max load (mm)	Average tensile strength (MPa)
PVA-2%-1	67.94	2.43	0.4635	2.54
PVA-2%-2	13.26	0.50	0.3094	
PVA-2%-3	114.56	4.04	0.6214	
PVA-2%-6	107.79	3.60	0.7377	
PVA-2%-7	59.53	2.12	0.9301	

Table 2.6 Tensile properties (PVA-3%)

ID	Maximum load (N)	Tensile strength (MPa)	Head displacement at max load (mm)	Average tensile strength (MPa)
PVA-3%-2	34.57	1.23	0.893	2.64
PVA-3%-3	111.52	3.13	2.094	
PVA-3%-4	67.22	2.48	1.122	
PVA-3%-5	60.38	2.38	0.758	
PVA-3%-7	118.67	4.16	2.343	
PVA-3%-8	58.79	2.48	0.216	

2.3.3 Number of Cracks

The number of cracks formed during the uniaxial tension tests for the PVA-2% and PVA-3% is presented in Table 2.7 and Table 2.8. The results indicate that, among the five specimens in the PVA-2%, three developed one crack each, while two developed two cracks. In contrast, the six specimens in the PVA-3% exhibited a different pattern, with three specimens developing one crack each and the remaining three developing three cracks.

Based on the results presented, the multiple crack rates for the PVA-2% and PVA-3% were calculated to be 0.4 and 0.5, respectively. While the rates are relatively similar, it is noteworthy that the maximum number of cracks observed in the PVA-2% was two, while the PVA-3% exhibited up to three cracks. This indicates that FRCC with a 3% fiber volume fraction (PVA-3%) is more susceptible to developing multiple cracks than FRCC with a 2% fiber volume fraction (PVA-2%).

Table 2.7 Number of cracks (PVA-2%)

ID	Number of cracks	Multiple cracks rate
PVA-2%-1	1	0.4
PVA-2%-2	1	
PVA-2%-3	1	
PVA-2%-6	2	
PVA-2%-7	2	

Table 2.8 Number of cracks (PVA-3%)

ID	Number of cracks	Multiple cracks rate
PVA-3%-2	1	0.5
PVA-3%-3	3	
PVA-3%-4	1	
PVA-3%-5	3	
PVA-3%-7	3	
PVA-3%-8	1	

2.3.4 Tensile Load-Head Displacement Relationship

The results of the tensile load-head displacement relationship obtained from the uniaxial tension test are shown in Figure 2.9 and Figure 2.10. The limited dimensions of the test specimens (test section with a cross-sectional area of 5 mm × 5 mm and a length of 30 mm) presented a significant challenge in the installation of a displacement gauge. Accordingly, the documented data pertains to the displacement of the head rather than the actual displacement of the test section. However, due to the limited dimensions of the specimens and the test section, it is assumed in this study that the head displacement is approximately equivalent to the total crack width.

From the experimental results, it was observed that in PVA-2%, the load increased gradually with head displacement, reaching a maximum load before gradually decreasing as head displacement continued to increase. In contrast, the PVA-3% displayed a distinct pattern: initially, the load increased with head displacement, reaching an initial peak. Subsequently, after reaching this peak, the load exhibited a slight decrease with further head displacement, followed by an increase. This cycle was repeated, demonstrating multiple crack behavior. The results indicate that the PVA-3% exhibited more pronounced multiple crack behavior compared to the PVA-2%. However, despite these differences in behavior, the maximum load values recorded for the PVA-3% and PVA-2% were similar.

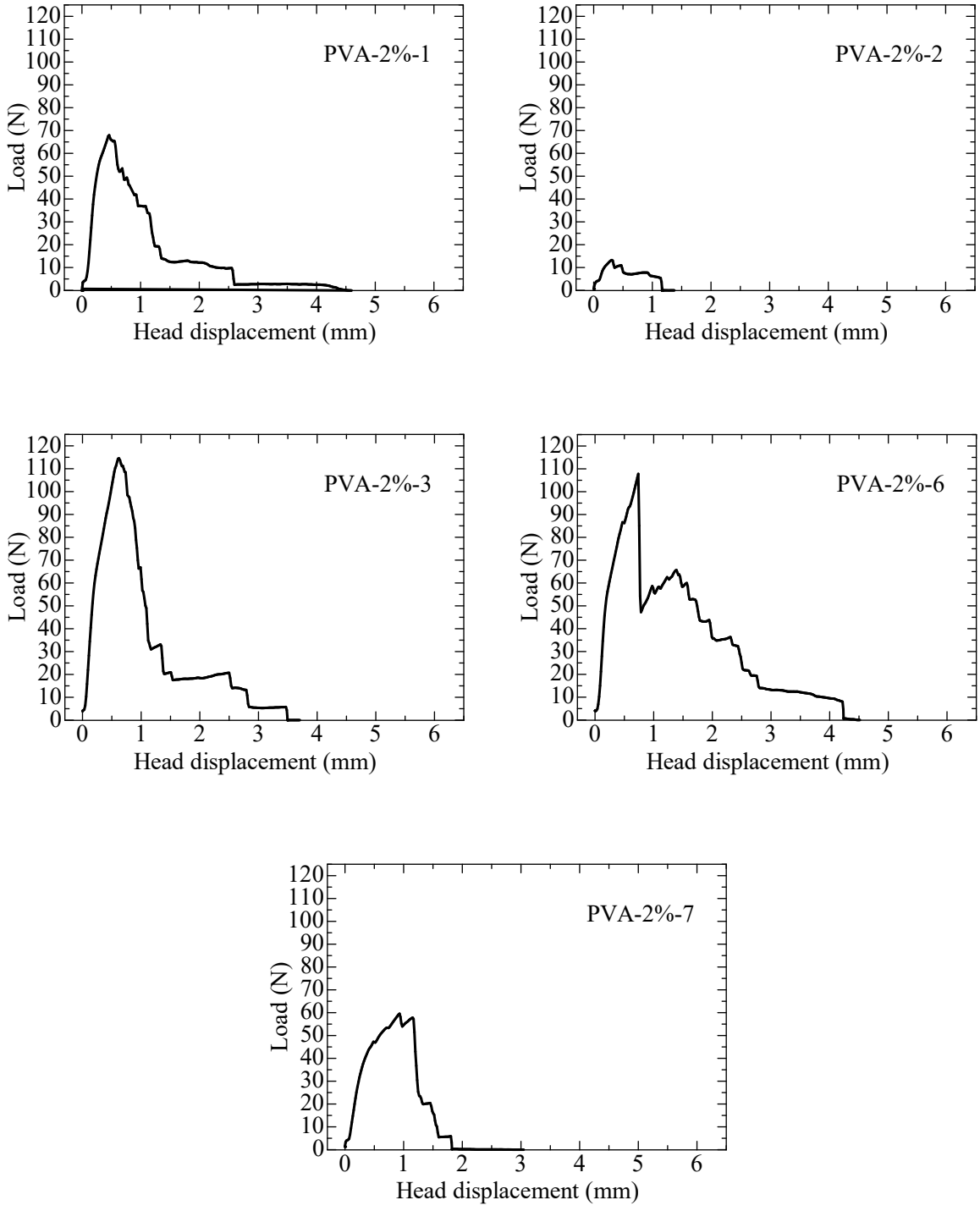

Figure 2.9 Tensile load-head displacement relationship (PVA-2%)

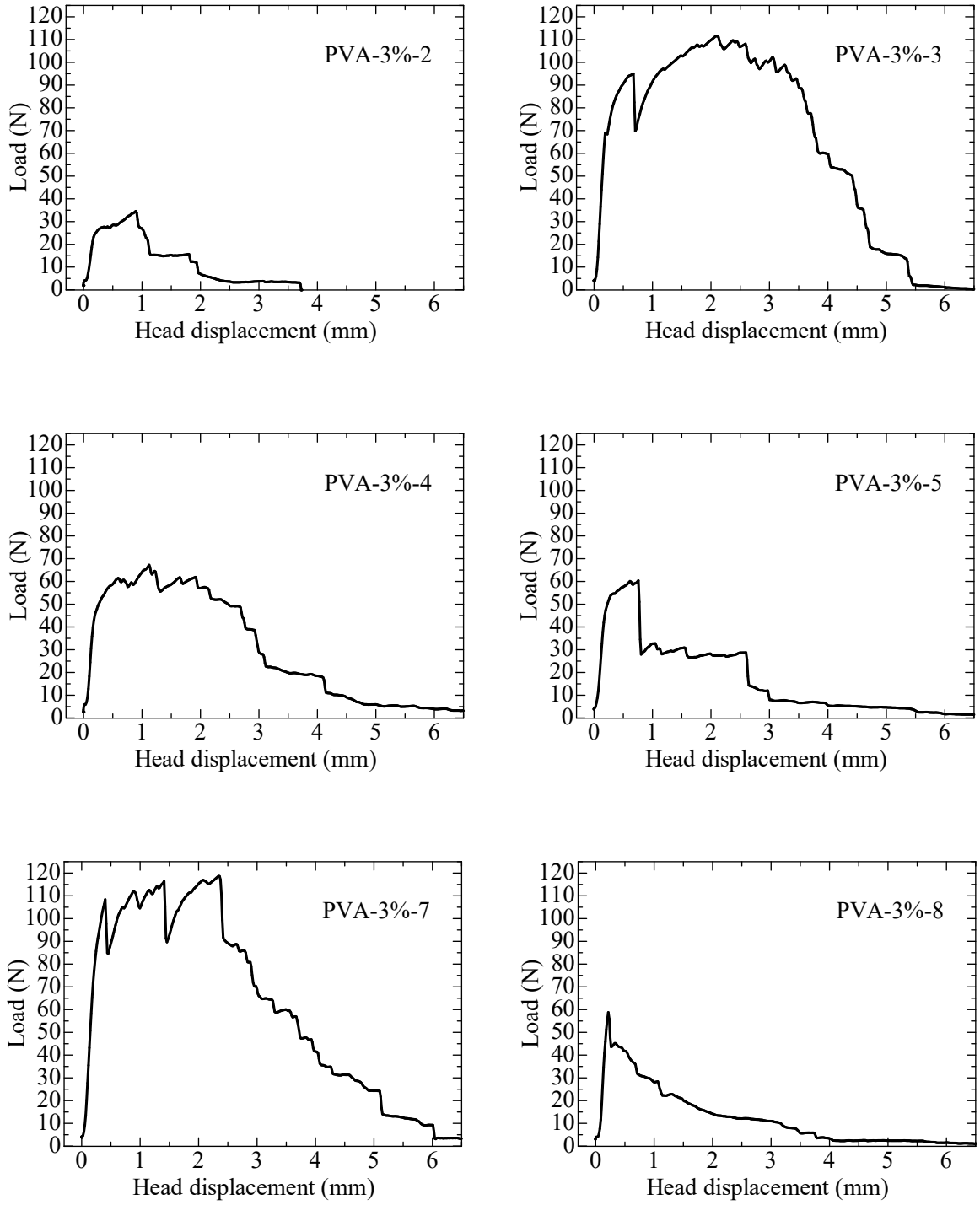

Figure 2.10 Tensile load-head displacement relationship (PVA-3%)

Chapter 3 Calculation of Bridging Law

3.1 Introduction

In this chapter, the bridging stress-crack width relationship is calculated using the PVA single fiber pullout model proposed in previous studies, under the condition that fiber orientation is excluded. The probability of fiber rupture is also considered, given that rupture may occur during the tensile process. Subsequently, the calculated results are compared with the experimental results. Moreover, a Monte Carlo simulation is utilized to assess the variability and potential errors in the calculated results. Finally, an investigation is conducted into the relationship between the fiber rupture probability in the computational model and the target bridging strength.

3.2 Tri-Linear Bridging Model for PVA Fiber

To compute the bridging stress-crack width relationship for the specimens, it is necessary to utilize the single fiber pullout model. In this study, the tri-linear bridging model was utilized to examine the pullout behavior of PVA single fiber, as shown in Figure 3.1.

The tri-linear bridging model subdivides the pullout behavior of PVA fibers into three stages. In the first stage, the hydroxyl groups present in PVA fiber form robust hydrogen intermolecular bonds, thereby facilitating the formation of a highly stable chemical bond between the PVA fiber and the hydration products of cement［9］. This chemical bond is the primary determinant of behavior between the 0-pullout load and the first peak bonding load, denoted as P_a.

Subsequently, the chemical bonding stage is followed by the friction stage, during which the matrix surrounding the fiber gradually separates from the fiber. The debonding process continues until the debonded length is equal to the fiber's embedded length, at this point, the pullout load reaches its maximum value［10］, denoted as P_{max}.

The final stage is the slippage stage, during which the fiber gradually pulls out while encountering resistance due to the frictional forces between the fiber and the surrounding matrix［10］. During this stage, the pullout load decreases steadily as the fiber is extracted, reaching zero when the fiber is completely pulled out.

In a previous study, a single pullout model for PVA fiber with a diameter of 0.1 mm and a length of 12 mm was established［11］. As the fiber dimensions utilized in this experiment are consistent with those from the prior research, the parameters for the single fiber pullout model applied in this study are presented in Table 3.1.

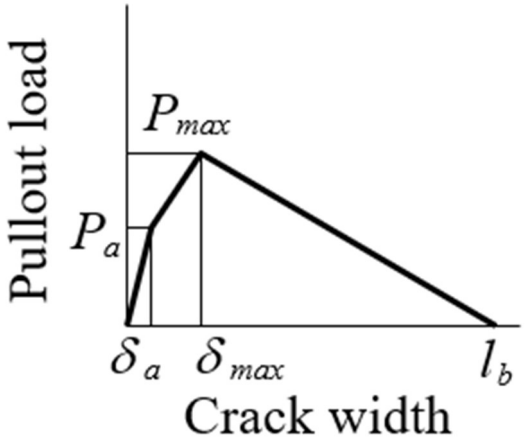

Figure 3.1 Tri-linear bridging model for PVA fiber

Table 3.1 Parameters for bridging law of PVA ［11］

Parameter	Input value
First peak load P_a (N)	1.5
Crack width at P_a, δ_a, (mm)	0.2
Maximum load P_{max} (N)	3.0
Crack width at P_{max}, δ_{max} (mm)	0.45

3.3 Calculation Method

In this study, the influence of fiber orientation is excluded, thereby rendering the embedded length of individual fibers the sole factor affecting single-fiber pullout behavior, as shown in Figure 3.2. Following the established criteria within the designated test area (cross-sectional area of 5 mm × 5 mm and length of 30 mm), the fibers (diameter 0.1 mm, length 12 mm) are distributed uniformly within the matrix. Due to the limitations of the test area, the orientation of the fibers remained fixed and aligned with the direction of the test area.

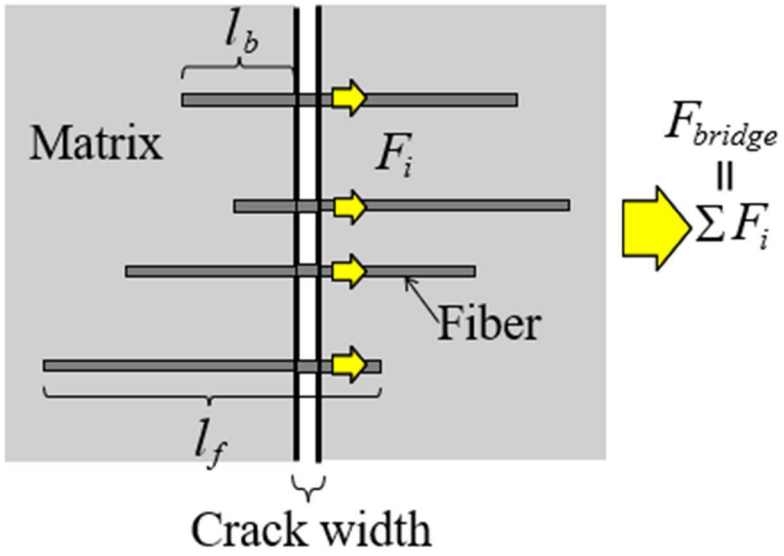

Figure 3.2 Calculation model

Therefore, when cracks emerged within the test area, the fibers that bridged across the cracks played a pivotal role in load transfer. However, as the fibers are oriented in alignment with the test area, the single-fiber pullout behavior is exclusively determined by the embedded length of the individual fibers. Following this supposition, Equation (1) and the calculated bridging force are employed. In this experiment, the fiber exhibited not only pullout behavior but also partial rupture during the tensile process. Despite the exclusion of fiber orientation in this study, the sound of fiber rupture was observed during the tests. The rupture of the fiber is caused by the bridging strength exceeding the apparent strength of the respective fiber.

Consequently, the probability of fiber rupture is taken into account during the pullout process, as rupturing sounds are detected during the experiments. Accordingly, Equation (1) incorporates a parameter for the probability of fiber rupture. For fibers that do not rupture during pullout, the pullout force is calculated using the tri-linear bridging model [11]. In the calculations, the value of P_r is determined by adjusting it so that the calculated bridging force closely matches the target load (= the maximum load for each specimen). This approach ensures that the calculated bridging force is as closely aligned with the experimentally observed maximum load for each specimen as is feasible. In the case of ruptured fibers, the pullout force is set to zero. The total bridging force within the test area is then obtained by summing the pullout forces of all fibers. The primary influencing factor in Equation (1) is the fiber rupture probability, denoted as P_r. Different P_r values result in varying bridging forces. The number of fibers within the test area is determined using Equation (2).

$$F_{bridge} \equiv \sum_{l_b \le l_{f/2}} \begin{cases} F_i(l_b) & (P > P_r) \\ 0 & (P \le P_r) \end{cases} \qquad (1)$$

$$P_r = f(n)$$

F_{bridge}: bridging force;
$F_i(l_b)$: pullout force of single fiber
P_r: fiber rupture probability;
l_b: embedded length;
l_f: fiber length;
n : assumed number for calculation.

$$N_f = V_f \times \frac{A_m}{A_f} \quad (2)$$

N_f: calculated number of fibers;

V_f: fiber volume fraction;

A_m: cross-sectional area of the specimen;

A_f: cross-sectional area of fiber.

3.4 Calculation Result

3.4.1 Monte Carlo Simulation

The results of this calculation method are contingent upon the occurrence of fiber rupture, which is itself influenced by differences in embedded lengths. Accordingly, Monte Carlo simulation (MCS) is utilized to examine the variability of the results. Each experimental result is subjected to 600 trials. The results for the PVA-2% and PVA-3% are presented in Figure 3.3 and Figure 3.4, respectively. The x-axis represents the number of trials, while the y-axis indicates the bridging strength (=maximum bridging force obtained in each calculation trial).

The bridging strength obtained by Monte Carlo simulation for the PVA-2% and PVA-3% is presented in Table 3.2 and Table 3.3, respectively. The standard deviation (SD) for the PVA-2% ranges from 0.54 N to 2.92 N. However, except for specimen PVA-2%-2, the SD for all other specimens falls within the range of 2 N to 3 N. This is attributed to the fact that the target calculated load for PVA-2%-2 is relatively small, at only 13.26N. Similarly, the SD for the PVA-3% ranges from 1.36 N to 4.13 N. As with the PVA-2%, the SD for all other specimens exceeds 2 N, except PVA-3%-2. This is also due to the small target calculated load for PVA-3%-2.

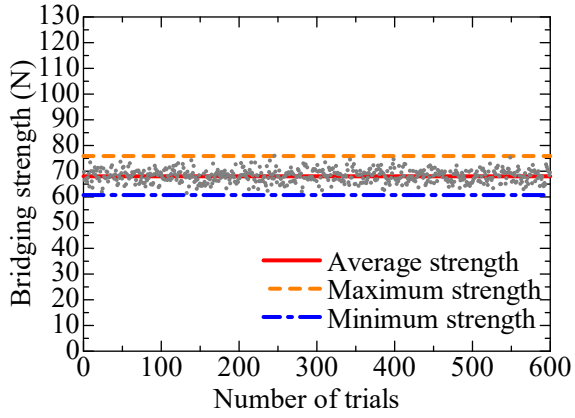

(a) PVA-2%-1

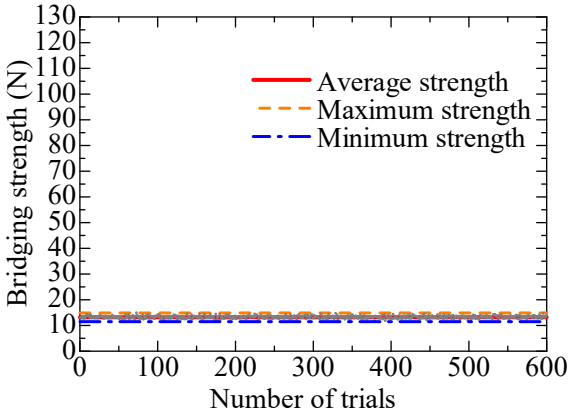

(b) PVA-2%-2

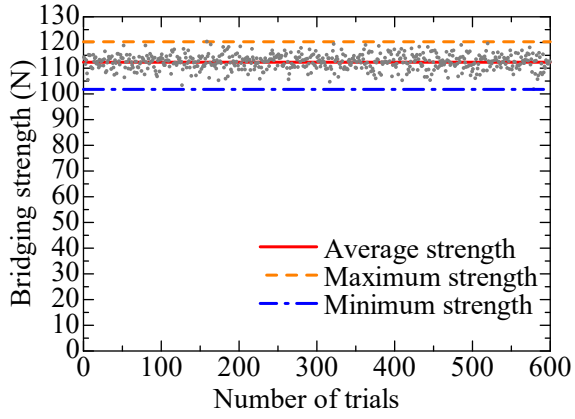

(c) PVA-2%-3

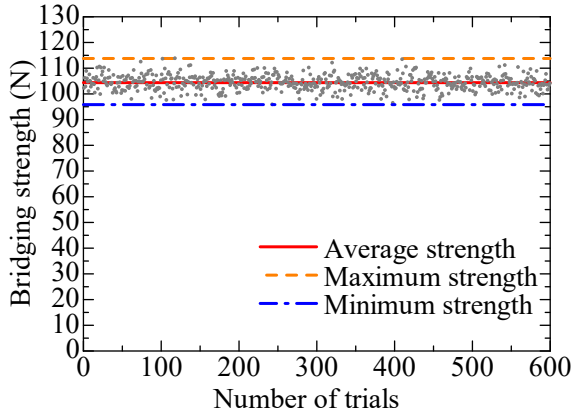

(d) PVA-2%-6

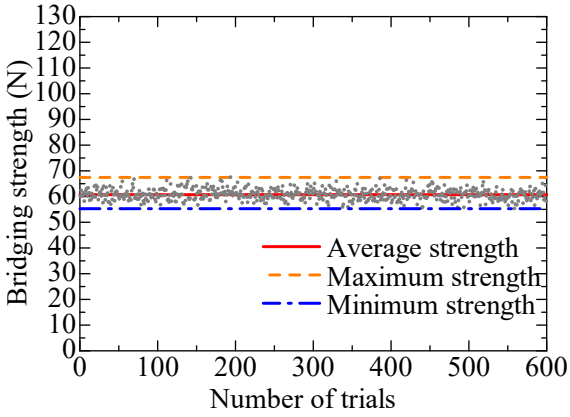

(e) PVA-2%-7

Figure 3.3 Bridging strength obtained by MCS (PVA-2%)

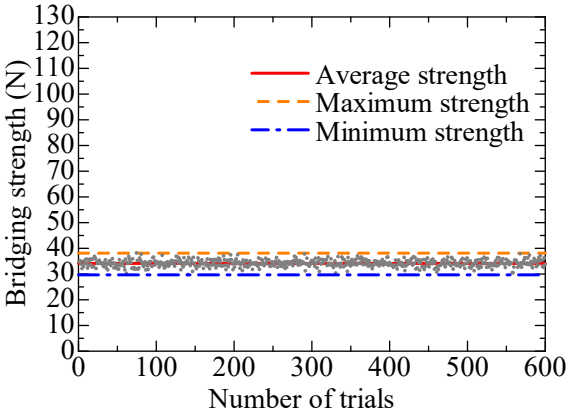

(a) PVA-3%-2

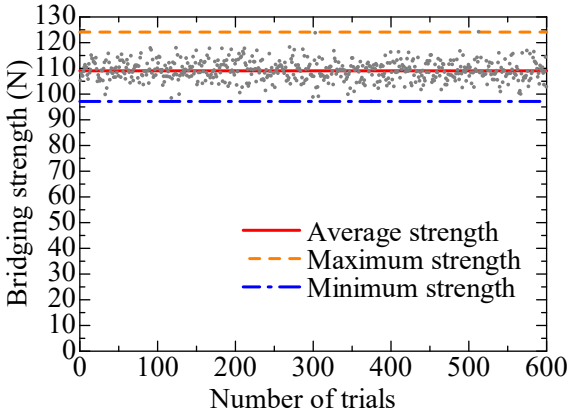

(b) PVA-3%-3

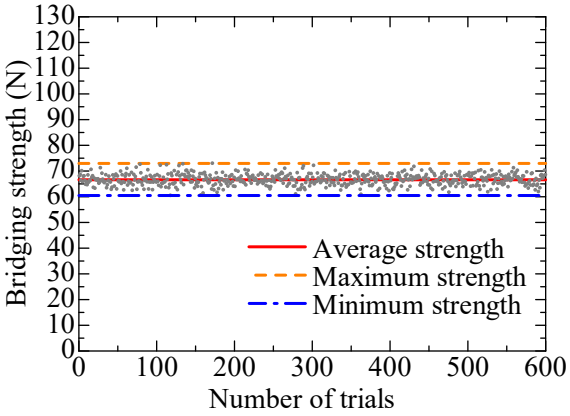

(c) PVA-3%-4

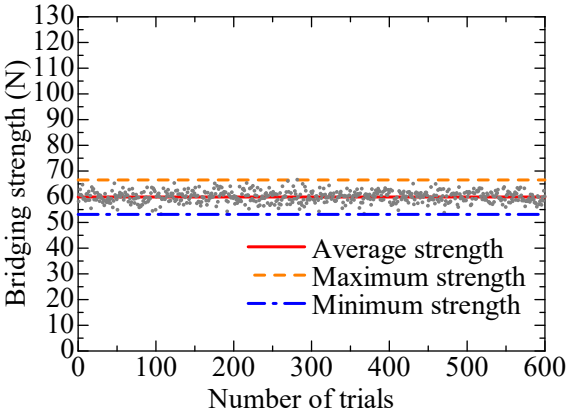

(d) PVA-3%-5

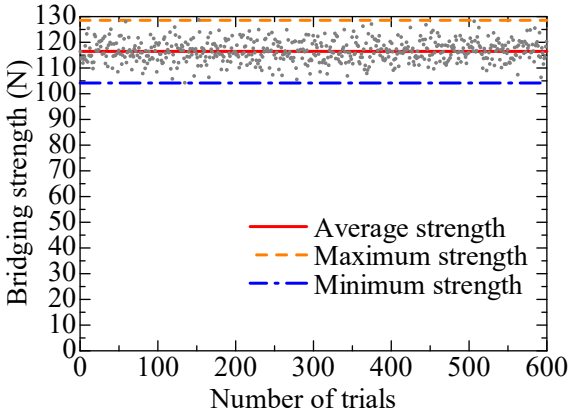

(e) PVA-3%-7

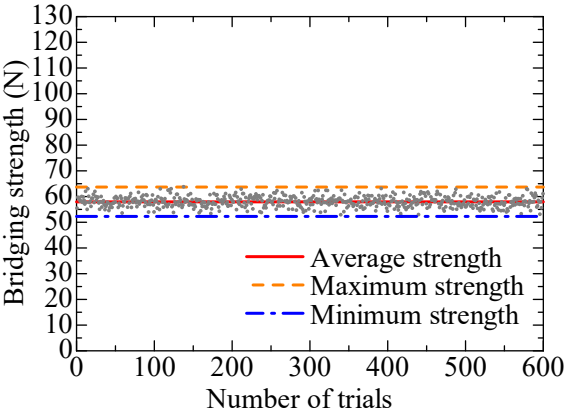

(f) PVA-3%-8

Figure 3.4 Bridging strength obtained by MCS (PVA-3%)

Table 3.2 Bridging strength obtained by Monte Carlo simulation (PVA-2%)

ID	Monte Carlo simulation (N)				
	P_r	Ave.	SD	Max.	Min.
PVA-2%-1	0.013	68.03	2.50	75.89	60.72
PVA-2%-2	0.077	13.18	0.54	14.87	11.48
PVA-2%-3	0.006	112.32	2.86	120.27	101.77
PVA-2%-6	0.007	104.38	2.92	113.78	95.84
PVA-2%-7	0.015	60.74	2.15	67.44	55.27

Table 3.3 Bridging strength obtained by Monte Carlo simulation (PVA-3%)

ID	Monte Carlo simulation (N)				
	P_r	Ave.	SD	Max.	Min.
PVA-3%-2	0.045	34.14	1.36	38.13	29.69
PVA-3%-3	0.012	109.04	3.82	124.13	97.13
PVA-3%-4	0.022	66.60	2.17	72.96	60.47
PVA-3%-5	0.025	59.90	2.16	66.54	53.13
PVA-3%-7	0.011	116.47	4.13	128.56	104.17
PVA-3%-8	0.026	57.94	2.07	63.70	52.27

3.4.2 Bridging Force-Crack Width Relationship

Each experimental result was subjected to 600 calculations, and the bridging force-crack width relationship for the PVA-2% and PVA-3% is illustrated in Figure 3.5 and Figure 3.6, respectively. In these figures, the red curve represents the maximum strength, defined as the highest bridging strength among the 600 calculation results. The blue curve represents the minimum strength, defined as the lowest bridging strength among the 600 calculation results. The gray curves correspond to the remaining 598 Monte Carlo simulations. The results demonstrate that the shape of the bridging force-crack width relationship curves for both the PVA-2% and PVA-3% closely resembles that of the tri-linear bridging model.

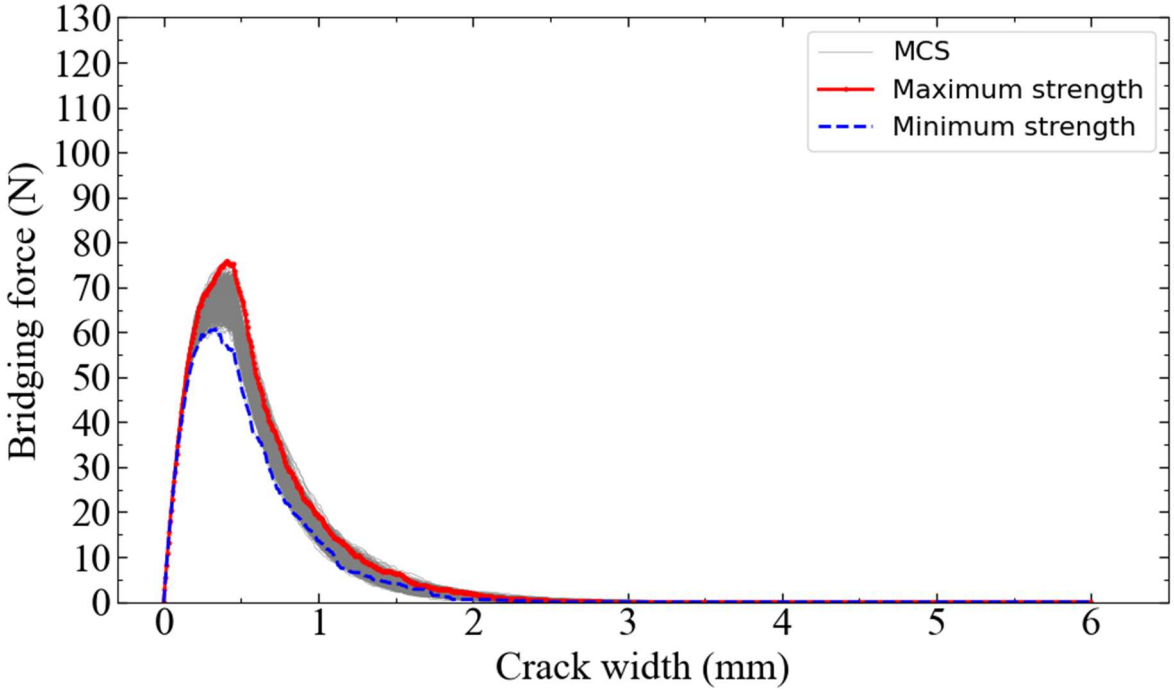

(a) PVA-2%-1

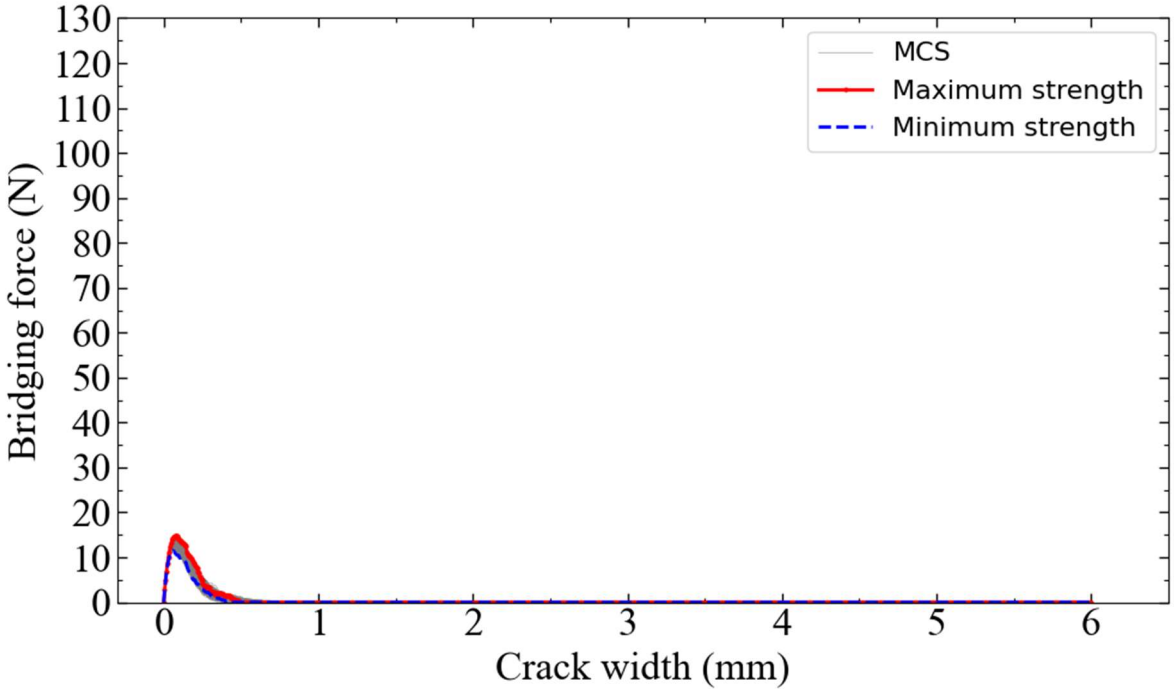

(b) PVA-2%-2

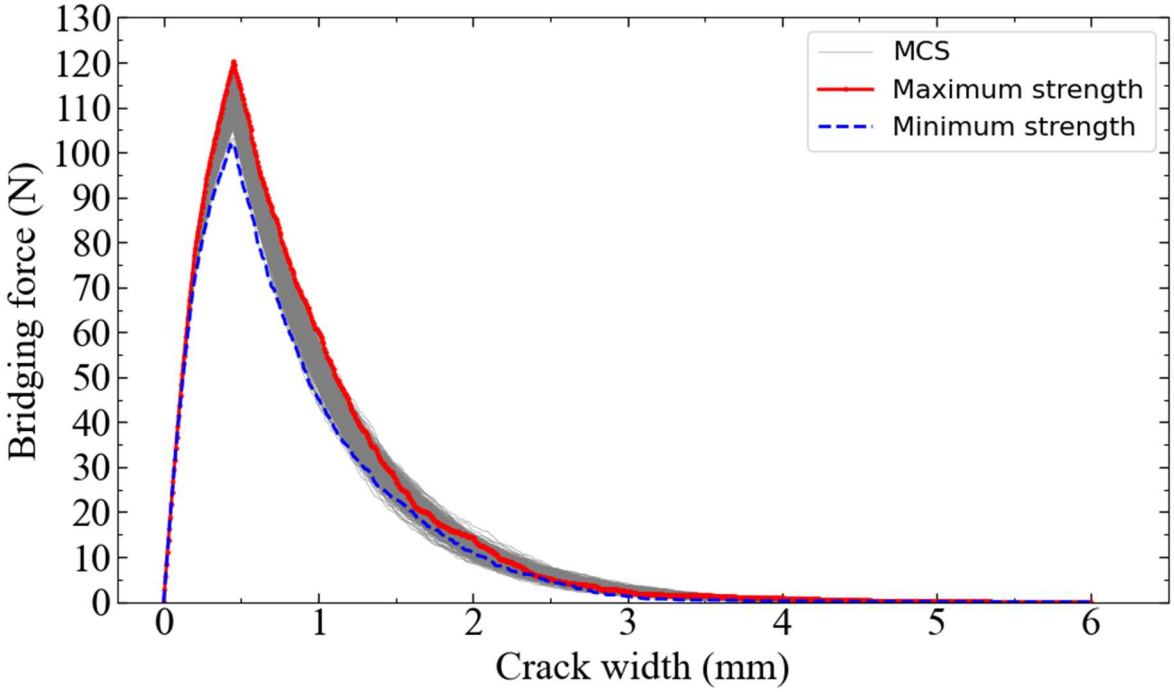

(c) PVA-2%-3

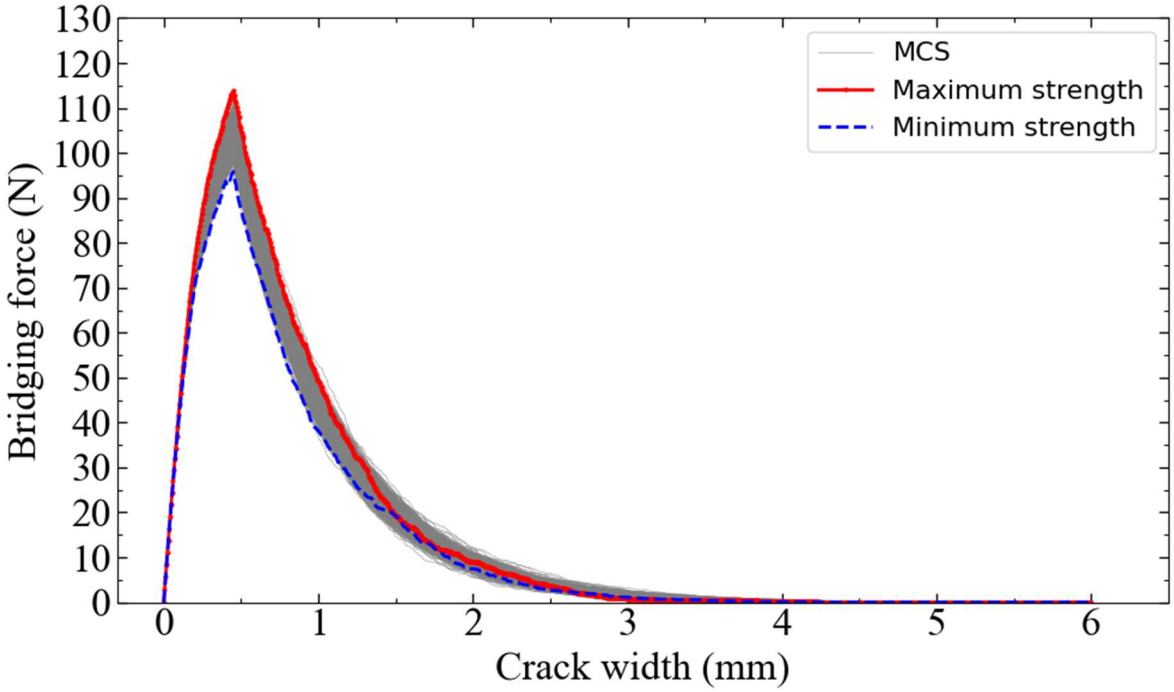

(d) PVA-2%-6

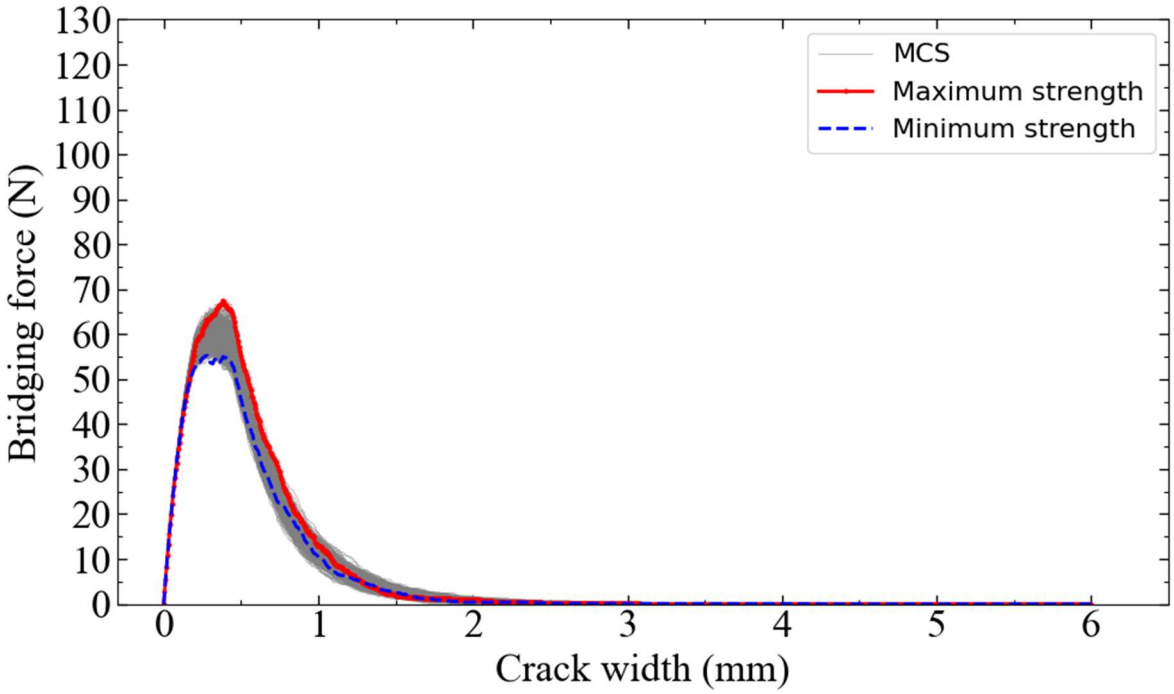

(e) PVA-2%-7

Figure 3.5 Bridging force-crack width relationship (PVA-2%)

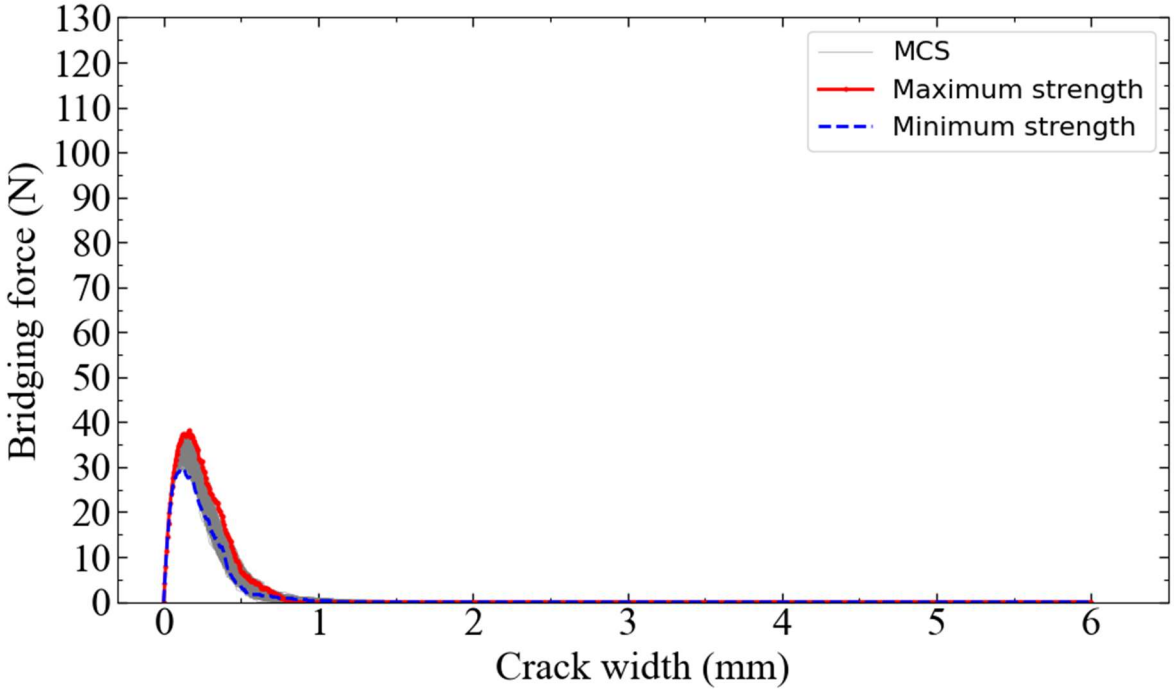

(a) PVA-3%-2

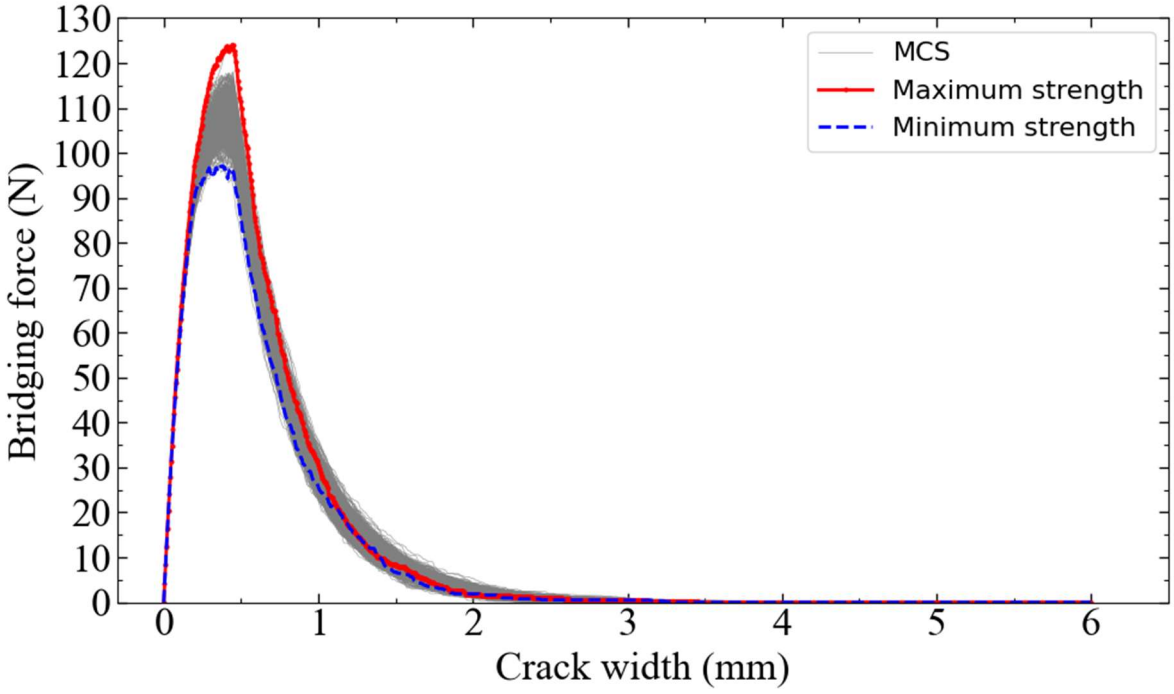

(b) PVA-3%-3

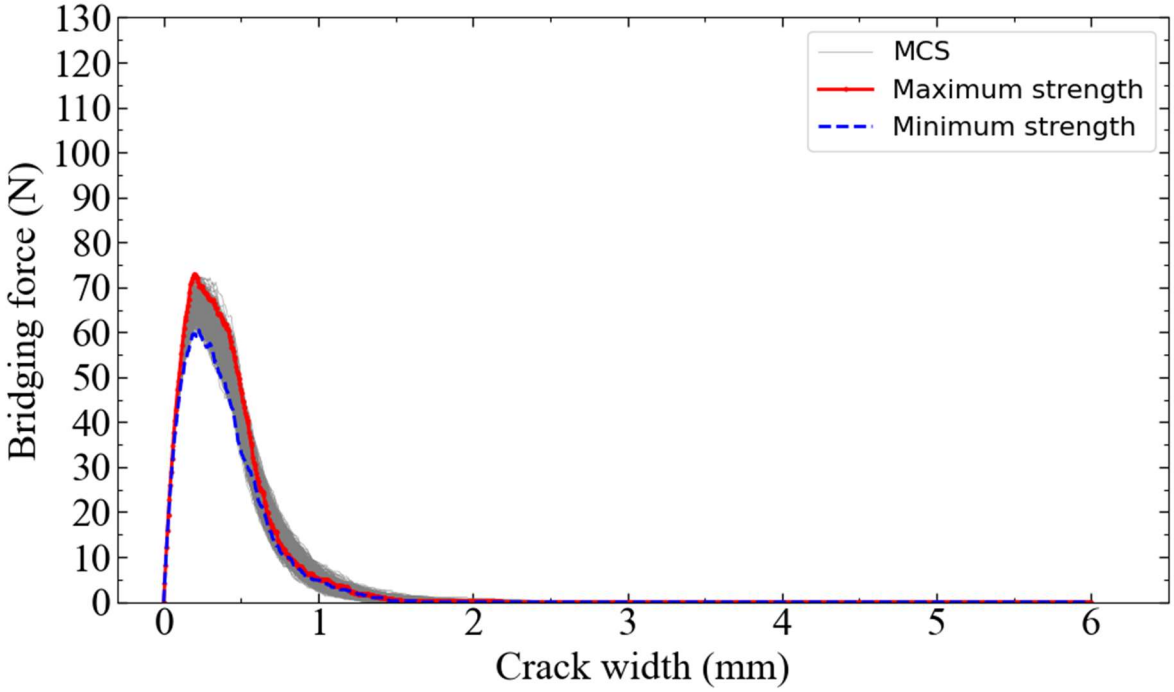

(c) PVA-3%-4

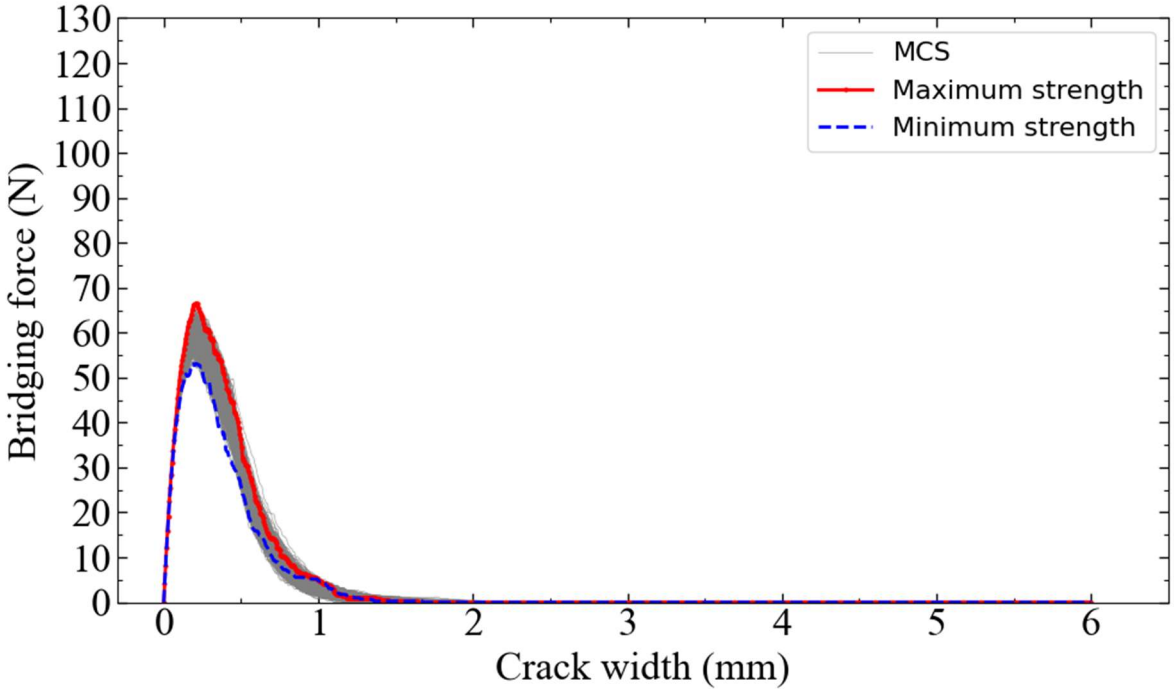

(d) PVA-3%-5

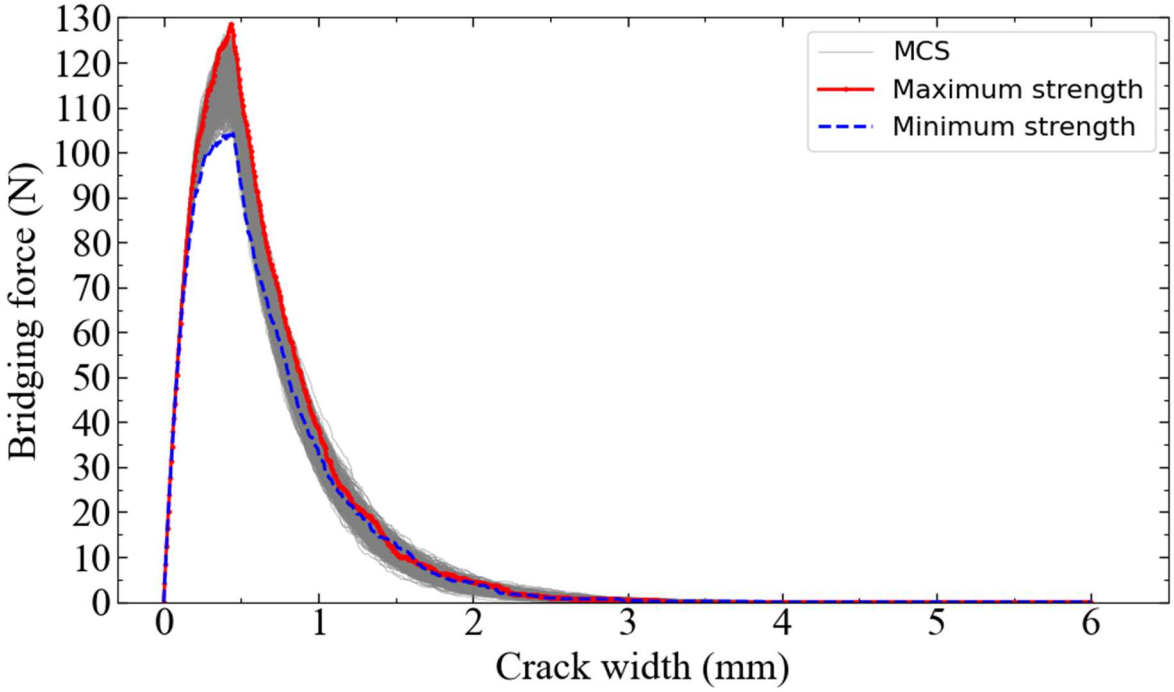

(e) PVA-3%-7

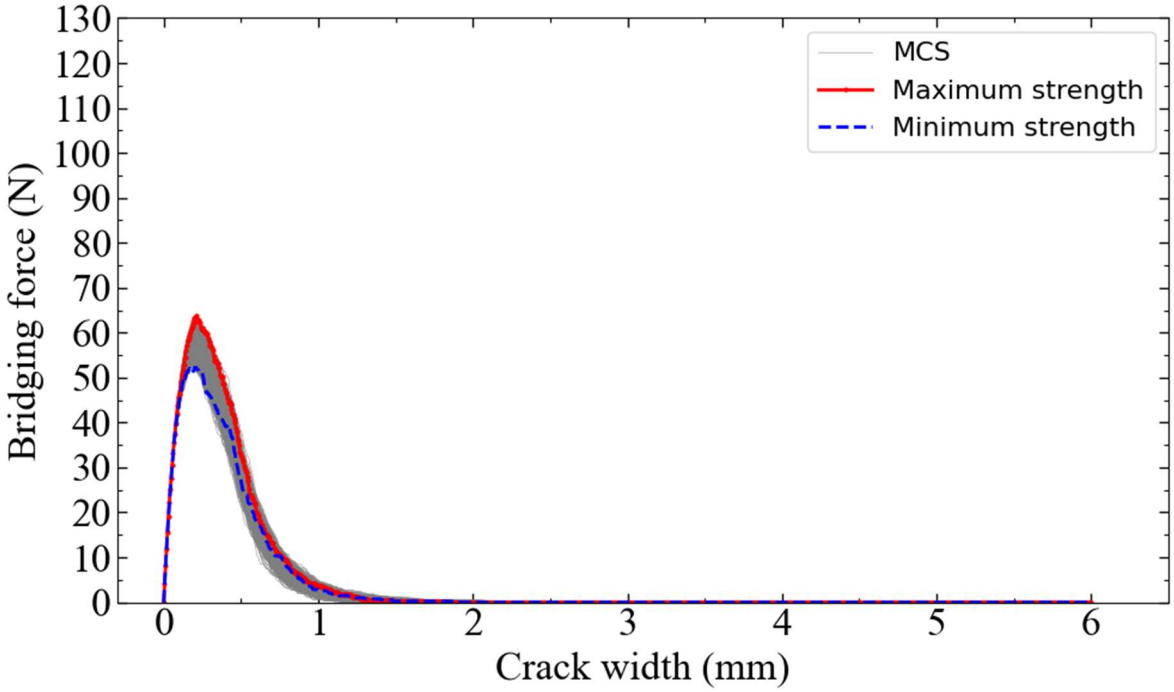

(f) PVA-3%-8

Figure 3.6 Bridging force-crack width relationship (PVA-3%)

3.4.3 Comparison of Calculation and Experimental Results

The comparison of calculation and experimental results for the PVA-2% and PVA-3% is presented in Figure 3.7 and Figure 3.8, respectively. As illustrated in the figures, the calculated results for the PVA-2% are in close agreement with the experimental results. While some specimens in the PVA-2% exhibited multiple crack behavior, the overall load-crack width relationship curve closely resembles the tri-linear bridging model, indicating a good fit between the calculated and experimental results.

However, the PVA-3% exhibited more pronounced multiple crack behavior, resulting in a more fluctuating curve. While the calculated bridging force is relatively close to the experimental maximum load, the fit of the curves is not as good. This suggests that the current calculation method may not be optimal for specimens exhibiting multiple crack behavior.

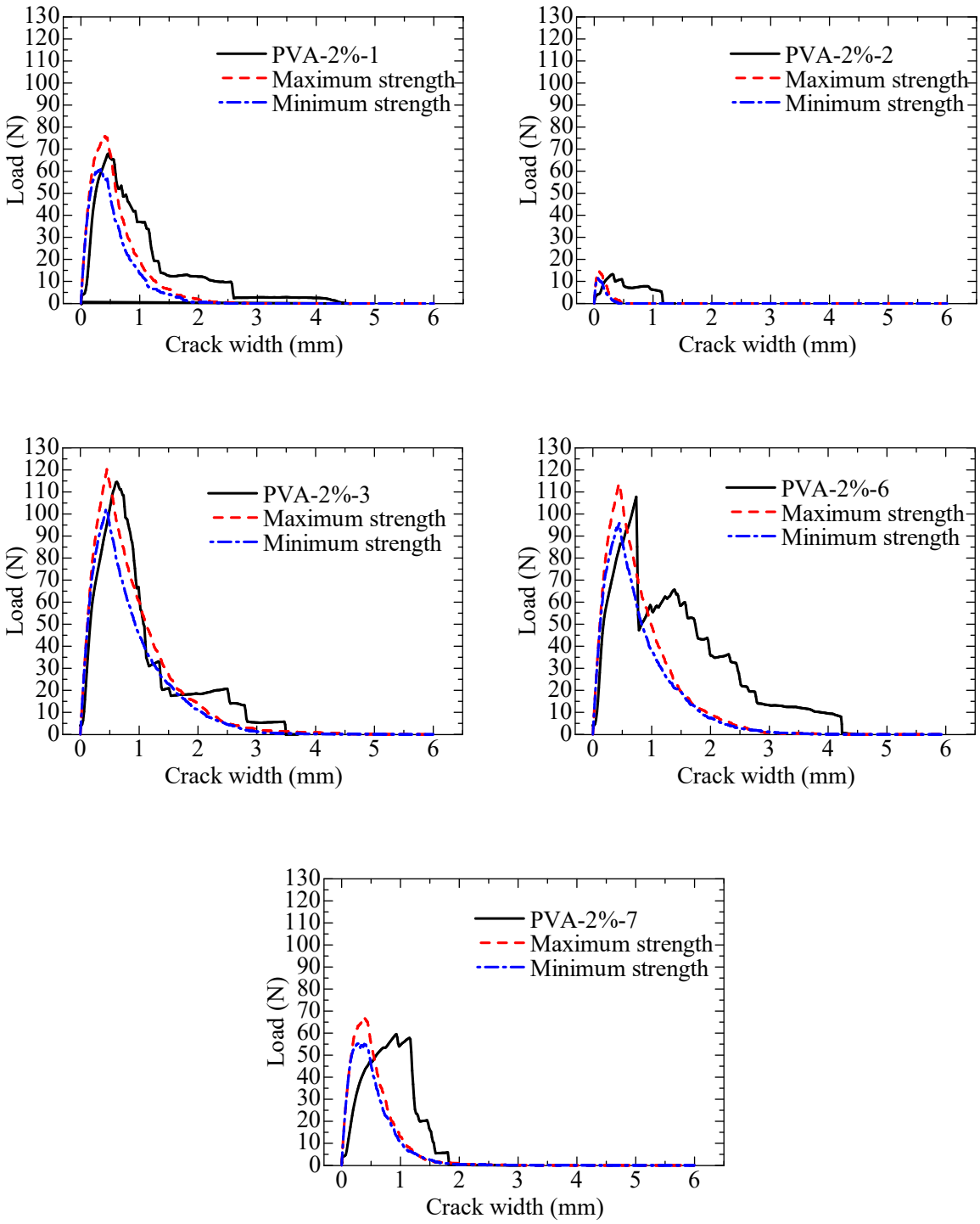

Figure 3.7 Comparison of calculation and experimental results (PVA-2%)

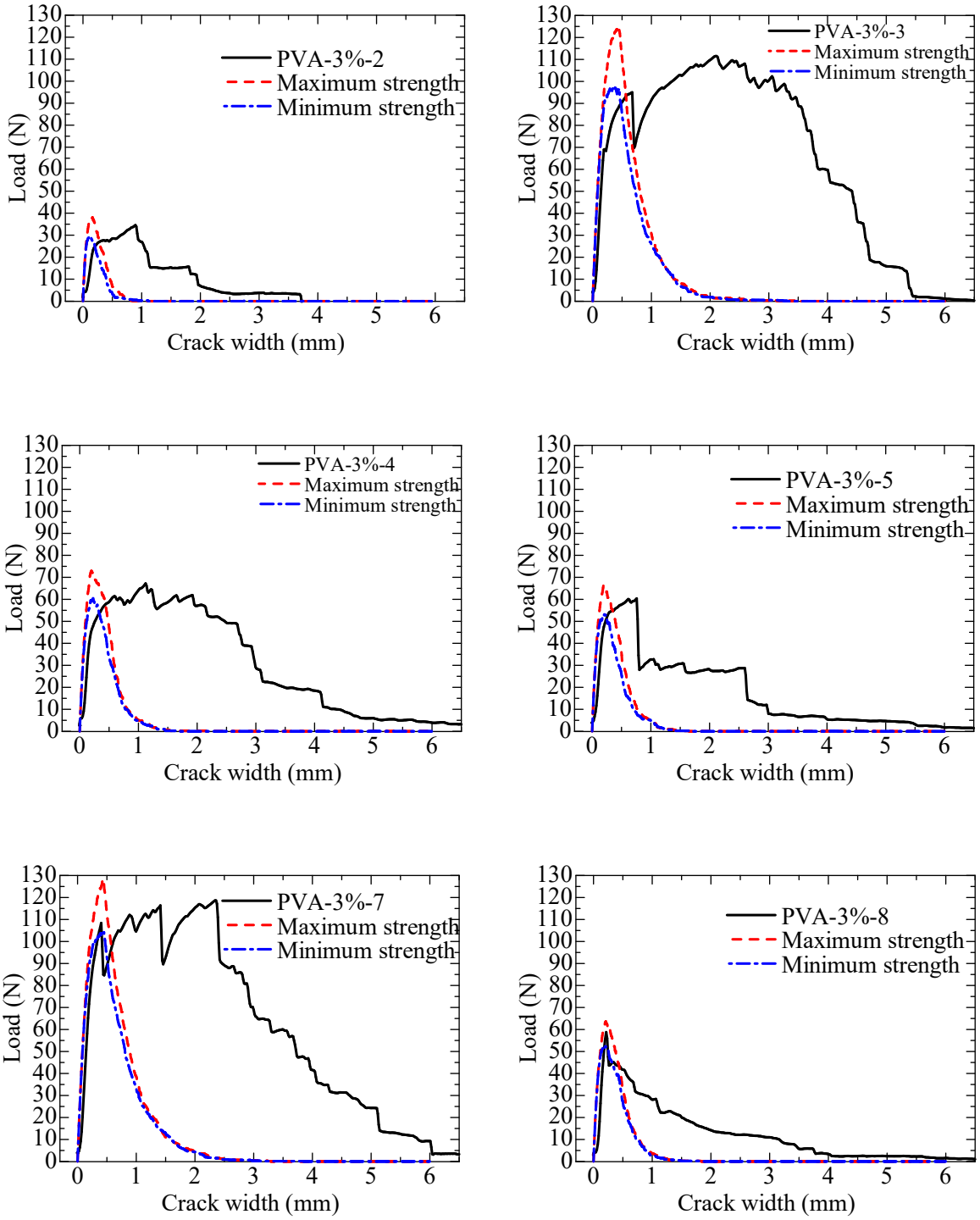

Figure 3.8 Comparison of calculation and experimental results (PVA-3%)

3.5 P_r-Target Load Relationship

The value of the fiber rupture probability (P_r) was determined based on the target load (= the maximum load for each specimen) by adjusting the calculated bridging force to closely match the target load. The target strength, calculation results, and the P_r values utilized are summarized in Table 3.4 and Table 3.5.

The results of the calculations demonstrate that the bridging strength is in close alignment with the target load for both the PVA-2% and PVA-3%. While the average value of P_r for both series is 0.024, the median values differ, with 0.013 for the PVA-2% and 0.024 for the PVA-3%. This indicates a considerable degree of variation in the values of P_r. The relationship between P_r and the target load is shown in Figure 3.9, in which R^2, the coefficient of determination, demonstrates a strong correlation between the derived equation and the experimental data. This suggests that the derived relationship accurately captures the connection between P_r and the target load.

Table 3.4 Calculation result (PVA-2%)

ID	Target load (N)	Bridging strength	P_r
PVA-2%-1	67.94	68.03	0.013
PVA-2%-2	13.26	13.18	0.077
PVA-2%-3	114.56	112.32	0.006
PVA-2%-6	107.79	104.38	0.007
PVA-2%-7	59.53	60.74	0.015
Ave.	72.62	71.73	0.024
Med.	67.94	68.03	0.013

Table 3.5 Calculation result (PVA-2%)

ID	Target load (N)	Bridging strength	P_r
PVA-3%-2	34.57	34.14	0.045
PVA-3%-3	111.52	109.04	0.012
PVA-3%-4	67.22	66.60	0.022
PVA-3%-5	60.38	59.90	0.025
PVA-3%-7	118.67	116.47	0.011
PVA-3%-8	58.79	57.94	0.026
Ave.	75.19	74.02	0.024
Med.	63.80	63.25	0.024

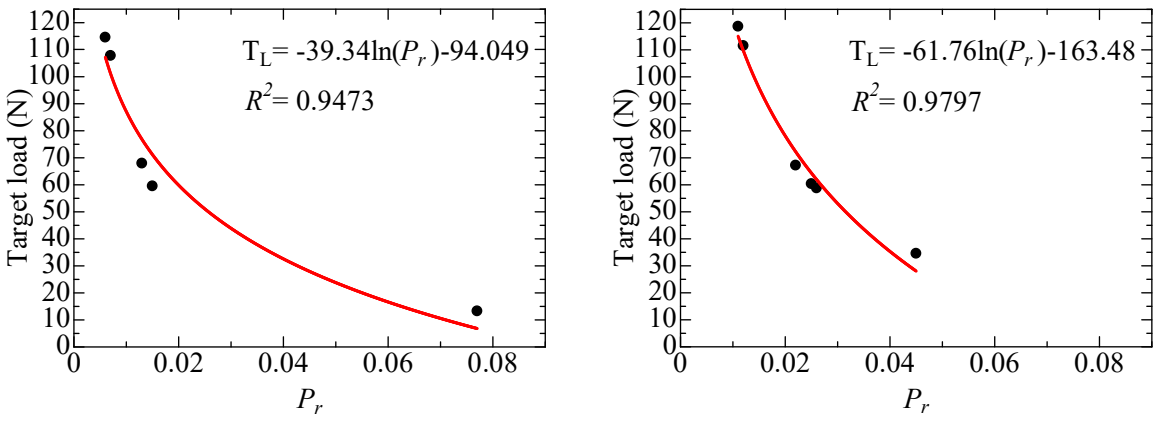

(a) PVA-2% (b) PVA-3%

Figure 3.9 P_r-target load relationship

Chapter 4 Conclusion

The objective of this study is to investigate the single-fiber pullout behavior of thin fibers. To this end, a uniaxial tension test was conducted on FRCC specimens with a minimal test area. By limiting the dimensions of the test area, the impact of fiber orientation is eliminated. Furthermore, the study employed a single-fiber pullout model for PVA fiber, taking into consideration the probability of fiber rupture, to assess the suitability of the proposed experimental method for evaluating the single-fiber pullout behavior of thin fibers. Based on the results, the following conclusions were drawn:

1. The results of the uniaxial tension test exhibit considerable variability. This variability can be attributed to the inherent large scatter in the tensile properties of cementitious materials, which is further amplified by the relatively small test area employed in this study.

2. In the fiber volume fraction range of 2% to 3%, both 2% and 3% specimens exhibited multiple crack behavior, with the 3% specimens displaying a greater number of cracks. Moreover, the tensile load–head displacement relationship curves revealed that PVA-2% predominantly exhibited single crack behavior, whereas PVA-3% demonstrated more pronounced multiple crack behavior. It can thus be concluded that PVA-FRCC, with a fiber volume fraction of 3% is more susceptible to multiple cracking than that with a fiber volume fraction of 2%.

3. The calculated bridging force–crack width relationships were employed for comparison with the experimental results. The calculations demonstrated a high degree of correlation with the PVA-2%. However, the experimental results for the PVA-3% demonstrated a more pronounced occurrence of multiple crack behavior, which resulted in a less precise alignment with the calculated data.

4. The calculated bridging strengths are in close alignment with the experimental tensile strengths in the fiber rupture probability of 0.024 as average. The relationship between fiber rupture probability and bridging strength shows a strong correlation expressed by the derived equation.

Acknowledgments

First and foremost, I would like to extend my most heartfelt gratitude to my academic supervisor, Professor Toshiyuki Kanakubo, for his invaluable guidance and support throughout the selection of this research topic and the implementation of the experiments. I offer him my sincerest thanks.

I would also like to express my appreciation to my sub-supervisors, Professor Takashi Matsushima and Associate Professor Akira Yasojima, whose advice and assistance were instrumental in the smooth progression of this research. Additionally, I am deeply thankful to Mr. Kojima for his support in creating the molds for the specimens and his help during the experiments.

Finally, I would like to thank Kuraray Co., Ltd. for providing the fibers used in this study, which greatly contributed to the successful execution of the experiments.

References

［1］ UCHIDA Yuichi, KUNIEDA Minoru, ROKUGO Keitetsu; FRCC–Design and application in Japan, In: Proc. of 1st ACI-fib FRC Workshop, pp. 58-68, 2014

［2］ Y. Ozu, M. Miyaguchi, T. Kanakubo: Modeling of Bridging Law for PVA Fiber-Reinforced Cementitious Composite Considering Fiber Orientation, Journal of Civil Engineering and Architecture, Volume 12, Number 9, pp.651-661, 2018.9

［3］ 閑田徹志：高靭性繊維補強セメント材料の設計技術の現状，コンクリート工学，Vol.38, No.6, pp.9-16,2000

［4］ 浅野浩平, 金久保利之 : 高性能繊維補強セメント複合材料における短繊維の付着性状に関する研究：その 1:PVA 単繊維の付着実験，日本建築学会大会学術講演梗概集（北陸），A-1 材料施工, pp.821-822, 2010

［5］ Selamawit Fthanegest Abrha, Helen Negash Shiferaw, Toshiyuki Kanakubo: Bridging Behavior of Palm Fiber in Cementitious Composite, Journal of Composites Science, Vol.8, No.9, 361 (23pp.), September 2024

［6］ Kanakubo, T., Shi, H., Wang, J.: Influence of Matrix Strength on Bridging Performance of Fiber-Reinforced Cementitious Composite with Bundled Aramid Fiber, Journal of Composites Science, Vol.6, No.5, 131, 2022.4

［7］ 橋本裕子，牟 雨，山田 大，金久保利之： FRCC におけるアラミドおよび PP 短繊維の抜出し挙動と架橋則の構築, 日本コンクリート工学会コンクリート工学論文集, 第 28 巻, pp.103～111，2017.11

［8］ Saki Echizen, Toshiyuki Kanakubo: Study on pullout behavior of single steel fiber in SFRCC, Proceedings of The 2019 World Congress on Advances in Structural Engineering and Mechanics (ASEM19), 2019

［9］ Kanda, T., and Li, V. C., Interface Property and Apparent Strength of High-Strength Hydrophilic Fiber in Cement Matrix, Journal of Materials in Civil Engineering, ASCE, V.10, No.1, pp. 5-13, 1998

［10］ Redon, C., Li, V. C., Wu, C., Hoshiro, H., Saito, T., and Ogawa, A., Measuring and Modifying Interface Properties of PVA Fibers in ECC Matrix, ASCE Journal of Materials in Civil Engineering, Vol.13, No.6, pp.399-406, 2001

［11］ Toshiyuki Kanakubo, et al.: Influence of Fiber Orientation on Bridging Performance of Polyvinyl Alcohol Fiber-Reinforced Cementitious Composite, Materials Journal,113(2), pp.131-141, 2016